Extended Measurement of the Cosmic-Ray Electron and Positron Spectrum from 11 GeV to 4.8 TeV with the Calorimetric Electron Telescope on the International Space Station

O. Adriani *et al.* (CALET Collaboration)

Phys. Rev. Lett. **120**, 261102 — Published 25 June 2018

DOI: 10.1103/PhysRevLett.120.261102

Extended Measurement of Cosmic-ray Electron and Positron Spectrum from 11 GeV to 4.8 TeV with the Calorimetric Electron Telescope on the International Space Station

O. Adriani,[1,2] Y. Akaike,[3,4] K. Asano,[5] Y. Asaoka,[6,7,*] M.G. Bagliesi,[8,9] E. Berti,[1,2] G. Bigongiari,[8,9] W.R. Binns,[10] S. Bonechi,[8,9] M. Bongi,[1,2] P. Brogi,[8,9] J.H. Buckley,[10] N. Cannady,[11] G. Castellini,[12] C. Checchia,[13,14] M.L. Cherry,[11] G. Collazuol,[13,14] V. Di Felice,[15,16] K. Ebisawa,[17] H. Fuke,[17] T.G. Guzik,[11] T. Hams,[3,18] M. Hareyama,[19] N. Hasebe,[6] K. Hibino,[20] M. Ichimura,[21] K. Ioka,[22] W. Ishizaki,[5] M.H. Israel,[10] K. Kasahara,[6] J. Kataoka,[6] R. Kataoka,[23] Y. Katayose,[24] C. Kato,[25] N. Kawanaka,[26,27] Y. Kawakubo,[28] K. Kohri,[29] H.S. Krawczynski,[10] J.F. Krizmanic,[18,3] T. Lomtadze,[9] P. Maestro,[8,9] P.S. Marrocchesi,[8,9] A.M. Messineo,[30,9] J.W. Mitchell,[4] S. Miyake,[31] A.A. Moiseev,[32,18] K. Mori,[6,17] M. Mori,[33] N. Mori,[2] H.M. Motz,[34] K. Munakata,[25] H. Murakami,[6] S. Nakahira,[35] J. Nishimura,[17] G.A. de Nolfo,[36] S. Okuno,[20] J.F. Ormes,[37] S. Ozawa,[6] L. Pacini,[1,12,2] F. Palma,[15,16] P. Papini,[2] A.V. Penacchioni,[8,38] B.F. Rauch,[10] S.B. Ricciarini,[12,2] K. Sakai,[18,3] T. Sakamoto,[28] M. Sasaki,[18,32] Y. Shimizu,[20] A. Shiomi,[39] R. Sparvoli,[15,16] P. Spillantini,[1] F. Stolzi,[8,9] J.E. Suh,[8,9] A. Sulaj,[8,9] I. Takahashi,[40] M. Takayanagi,[17] M. Takita,[5] T. Tamura,[20] N. Tateyama,[20] T. Terasawa,[35] H. Tomida,[17] S. Torii,[6,7,41,†] Y. Tsunesada,[42] Y. Uchihori,[43] S. Ueno,[17] E. Vannuccini,[2] J.P. Wefel,[11] K. Yamaoka,[44] S. Yanagita,[45] A. Yoshida,[28] and K. Yoshida[46]

(CALET Collaboration)

[1] *Department of Physics, University of Florence, Via Sansone, 1 - 50019 Sesto, Fiorentino, Italy*
[2] *INFN Sezione di Florence, Via Sansone, 1 - 50019 Sesto, Fiorentino, Italy*
[3] *Department of Physics, University of Maryland, Baltimore County, 1000 Hilltop Circle, Baltimore, MD 21250, USA*
[4] *Astroparticle Physics Laboratory, NASA/GSFC, Greenbelt, MD 20771, USA*
[5] *Institute for Cosmic Ray Research, The University of Tokyo, 5-1-5 Kashiwa-no-Ha, Kashiwa, Chiba 277-8582, Japan*
[6] *Research Institute for Science and Engineering, Waseda University, 3-4-1 Okubo, Shinjuku, Tokyo 169-8555, Japan*
[7] *JEM Utilization Center, Human Spaceflight Technology Directorate, Japan Aerospace Exploration Agency, 2-1-1 Sengen, Tsukuba, Ibaraki 305-8505, Japan*
[8] *Department of Physical Sciences, Earth and Environment, University of Siena, via Roma 56, 53100 Siena, Italy*
[9] *INFN Sezione di Pisa, Polo Fibonacci, Largo B. Pontecorvo, 3 - 56127 Pisa, Italy*
[10] *Department of Physics, Washington University, One Brookings Drive, St. Louis, MO 63130-4899, USA*
[11] *Department of Physics and Astronomy, Louisiana State University, 202 Nicholson Hall, Baton Rouge, LA 70803, USA*
[12] *Institute of Applied Physics (IFAC), National Research Council (CNR), Via Madonna del Piano, 10, 50019 Sesto, Fiorentino, Italy*
[13] *Department of Physics and Astronomy, University of Padova, Via Marzolo, 8, 35131 Padova, Italy*
[14] *INFN Sezione di Padova, Via Marzolo, 8, 35131 Padova, Italy*
[15] *University of Rome "Tor Vergata", Via della Ricerca Scientifica 1, 00133 Rome, Italy*
[16] *INFN Sezione di Rome "Tor Vergata", Via della Ricerca Scientifica 1, 00133 Rome, Italy*
[17] *Institute of Space and Astronautical Science, Japan Aerospace Exploration Agency, 3-1-1 Yoshinodai, Chuo, Sagamihara, Kanagawa 252-5210, Japan*
[18] *CRESST and Astroparticle Physics Laboratory NASA/GSFC, Greenbelt, MD 20771, USA*
[19] *St. Marianna University School of Medicine, 2-16-1, Sugao, Miyamae-ku, Kawasaki, Kanagawa 216-8511, Japan*
[20] *Kanagawa University, 3-27-1 Rokkakubashi, Kanagawa, Yokohama, Kanagawa 221-8686, Japan*
[21] *Faculty of Science and Technology, Graduate School of Science and Technology, Hirosaki University, 3, Bunkyo, Hirosaki, Aomori 036-8561, Japan*
[22] *Yukawa Institute for Theoretical Physics, Kyoto University, Kitashirakawa Oiwakecho, Sakyo, Kyoto 606-8502, Japan*
[23] *National Institute of Polar Research, 10-3, Midori-cho, Tachikawa, Tokyo 190-8518, Japan*
[24] *Faculty of Engineering, Division of Intelligent Systems Engineering, Yokohama National University, 79-5 Tokiwadai, Hodogaya, Yokohama 240-8501, Japan*
[25] *Faculty of Science, Shinshu University, 3-1-1 Asahi, Matsumoto, Nagano 390-8621, Japan*
[26] *Hakubi Center, Kyoto University, Yoshida Honmachi, Sakyo-ku, Kyoto, 606-8501, Japan*
[27] *Department of Astronomy, Graduate School of Science, Kyoto University, Kitashirakawa Oiwake-cho, Sakyo-ku, Kyoto, 606-8502, Japan*

[28] *College of Science and Engineering, Department of Physics and Mathematics, Aoyama Gakuin University, 5-10-1 Fuchinobe, Chuo, Sagamihara, Kanagawa 252-5258, Japan*
[29] *Institute of Particle and Nuclear Studies, High Energy Accelerator Research Organization, 1-1 Oho, Tsukuba, Ibaraki, 305-0801, Japan*
[30] *University of Pisa, Polo Fibonacci, Largo B. Pontecorvo, 3 - 56127 Pisa, Italy*
[31] *Department of Electrical and Electronic Systems Engineering, National Institute of Technology, Ibaraki College, 866 Nakane, Hitachinaka, Ibaraki 312-8508 Japan*
[32] *Department of Astronomy, University of Maryland, College Park, Maryland 20742, USA*
[33] *Department of Physical Sciences, College of Science and Engineering, Ritsumeikan University, Shiga 525-8577, Japan*
[34] *International Center for Science and Engineering Programs, Waseda University, 3-4-1 Okubo, Shinjuku, Tokyo 169-8555, Japan*
[35] *RIKEN, 2-1 Hirosawa, Wako, Saitama 351-0198, Japan*
[36] *Heliospheric Physics Laboratory, NASA/GSFC, Greenbelt, MD 20771, USA*
[37] *Department of Physics and Astronomy, University of Denver, Physics Building, Room 211, 2112 East Wesley Ave., Denver, CO 80208-6900, USA*
[38] *ASI Science Data Center (ASDC), Via del Politecnico snc, 00133 Rome, Italy*
[39] *College of Industrial Technology, Nihon University, 1-2-1 Izumi, Narashino, Chiba 275-8575, Japan*
[40] *Kavli Institute for the Physics and Mathematics of the Universe, The University of Tokyo, 5-1-5 Kashiwanoha, Kashiwa, 277-8583, Japan*
[41] *School of Advanced Science and Engineering, Waseda University, 3-4-1 Okubo, Shinjuku, Tokyo 169-8555, Japan*
[42] *Division of Mathematics and Physics, Graduate School of Science, Osaka City University, 3-3-138 Sugimoto, Sumiyoshi, Osaka 558-8585, Japan*
[43] *National Institutes for Quantum and Radiation Science and Technology, 4-9-1 Anagawa, Inage, Chiba 263-8555, JAPAN*
[44] *Nagoya University, Furo, Chikusa, Nagoya 464-8601, Japan*
[45] *College of Science, Ibaraki University, 2-1-1 Bunkyo, Mito, Ibaraki 310-8512, Japan*
[46] *Department of Electronic Information Systems, Shibaura Institute of Technology, 307 Fukasaku, Minuma, Saitama 337-8570, Japan*

(Dated: May 21, 2018)

Extended results on the cosmic-ray electron + positron spectrum from 11 GeV to 4.8 TeV are presented based on observations with the CALET instrument on the International Space Station utilizing the data up to November 2017. The analysis uses the full detector acceptance at high energies, approximately doubling the statistics compared to the previous result. CALET is an all-calorimetric instrument with total thickness of 30 X_0 at normal incidence and fine imaging capability, designed to achieve large proton rejection and excellent energy resolution well into the TeV energy region. The observed energy spectrum in the region below 1 TeV shows good agreement with AMS-02 data. In the energy region below ∼300 GeV, CALET's spectral index is found to be consistent with AMS-02, Fermi-LAT and DAMPE, while from 300 GeV to 600 GeV the spectrum is significantly softer than the spectra from the latter two experiments. The absolute flux of CALET is consistent with other experiments at around a few tens of GeV. However, it is lower than those of DAMPE and Fermi-LAT with the difference increasing up to several hundred GeV. The observed energy spectrum above ∼1 TeV suggests a flux suppression consistent within the errors with the results of DAMPE, while CALET does not observe any significant evidence for a narrow spectral feature in the energy region around 1.4 TeV. Our measured all-electron flux including statistical errors and a detailed breakdown of the systematic errors is tabulated in the Supplemental Material, in order to allow more refined spectral analyses based on our data.

PACS numbers: 96.50.sb,95.35.+d,95.85.Ry,98.70.Sa,29.40.Vj

INTRODUCTION

High-energy cosmic-ray electrons provide a unique probe of nearby cosmic accelerators. Electrons rapidly lose energy via inverse Compton scattering and synchrotron emission during propagation in the galaxy. Since their diffusion distance above 1 TeV is less than 1 kpc, only a few potential TeV sources are expected in the vicinity of the solar system. A precise measurement of the electron spectrum in the TeV region might reveal interesting spectral features to provide the first experimental evidence of the possible presence of a nearby cosmic-ray source [1, 2]. In addition, the prominent increase of the positron fraction over 10 GeV established by PAMELA [3] and AMS-02 [4] may require a primary source component for positrons in addition to the generally accepted secondary origin. Candidates for such primary sources range from astrophysical (pulsar) to exotic (dark matter). Since these primary sources emit electron-positron pairs, it is expected that the all-electron (electrons + positrons) spectrum would exhibit a spectral feature, near the highest energy range of the primary component.

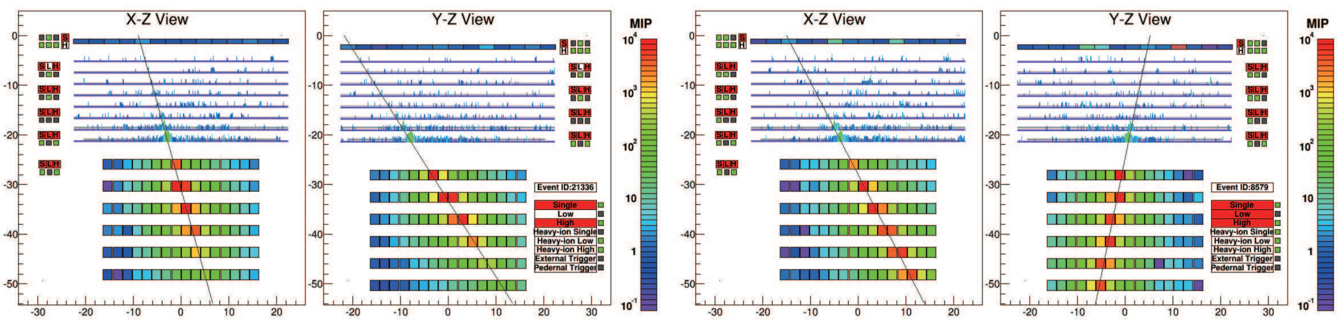

FIG. 1. Examples of TeV event candidates showing energy deposit in each detector channel in the X-Z and Y-Z views. Left-hand panel shows an electron (or positron) candidate (reconstructed energy of 3.05 TeV and energy deposit sum of 2.89 TeV), and the right-hand panel shows a proton candidate (energy deposit sum of 2.89 TeV).

The CALET collaboration managing the CALorimetric Electron Telescope (CALET) [5], a space-based instrument optimized for the measurement of the all-electron spectrum, published its first result in the energy range from 10 GeV to 3 TeV [6]. Subsequently, the DArk Matter Particle Explorer (DAMPE) collaboration published their all-electron spectrum in the energy range from 25 GeV to 4.6 TeV [7].

In this paper, we present an updated version of the CALET all-electron spectrum. Using 780 days of flight data from October 13, 2015 to November 30, 2017 and the full geometrical acceptance in the high energy region, we have increased our statistics by a factor of $\sim$2 compared to Ref. [6]. The energy range is also extended up to 4.75 TeV. Features of the spectrum measured by CALET are discussed, particularly in relation to the break reported by DAMPE at 0.9 TeV. The possible presence of a peak close to 1.4 TeV is tested with CALET data by using exactly the same energy binning as that of DAMPE. The systematic uncertainties are classified into several categories in order to allow for more sensitive interpretative studies using the CALET spectrum.

CALET INSTRUMENT

CALET employs a fully active calorimeter with 30 radiation-length thickness for particles at normal incidence. It consists of a charge detector (CHD), a 3 radiation-length thick imaging calorimeter (IMC) and a 27 radiation-length thick total absorption calorimeter (TASC), having a field of view of $\sim 45^\circ$ from zenith and a geometrical factor of $\sim$1040 cm^{2}sr for high-energy electrons.

CHD, which identifies the charge of the incident particle, is comprised of a pair of plastic scintillator hodoscopes arranged in two orthogonal layers. IMC is a sampling calorimeter alternating thin layers of Tungsten absorber, optimized in thickness and position, with layers of scintillating fibers read out individually. TASC is a tightly packed lead-tungstate ($PbWO_4$; PWO) hodoscope, capable of almost complete absorption of the TeV-electron showers. A more complete description of the instrument is given in the supplemental material of Ref. [6].

Figure 1 shows a 3.05 TeV electron candidate and a proton candidate with comparable energy deposit (2.89 TeV) in the detector. Compared to hadron showers which have significant leakage, the containment of the electromagnetic shower creates a difference in shower shape especially in the bottom part of TASC, allowing for an accurate electron identification in the presence of a large hadron background. Together with the precision energy measurements from total absorption of electromagnetic showers, it is possible to derive the electron spectrum well into the TeV region with a straightforward and reliable analysis.

The instrument was launched on August 19, 2015 and emplaced on the Japanese Experiment Module-Exposed Facility on the International Space Station (ISS) with an expected mission duration of five years (or more). Scientific observations [8] were started on October 13, 2015, and smooth and continuous operations have taken place since then.

DATA ANALYSIS

We have analyzed 780 days of flight data collected with a high-energy shower trigger [8]. Total live time in this period was 15,811 hours, corresponding to a live time fraction of 84%. The analysis was extended to use the full detector acceptance at higher energies as explained further down, otherwise it was done following the standard analysis procedure described in Ref. [6].

A Monte Carlo (MC) program was used to simulate physics processes and detector response based on the simulation package EPICS [9, 10] (EPICS9.20 / Cosmos8.00). Using MC event samples of electrons and protons, event selection and event reconstruction efficiencies, energy correction factor, and background contamination were derived. An independent analysis based on Geant4 [11] was performed, and small differences between the MC models are included in the systematic uncertainties. The detector model used in the Geant4 simulation is almost identical to the CALET CAD model. The Geant4 simulation employs the hadronic interaction models FTFP_BERT as physics list while DPMJET3 [12] is chosen as the hadronic interaction model in the EPICS simulation.

While excellent energy resolution inside the TeV region is one of the most important features of a thick calorimeter instrument like CALET or DAMPE, calibration errors must be carefully assessed and taken into account in the estimation of the actual energy resolution. Our energy calibration [13] includes the evaluation of the conversion factors between ADC units and energy deposits, ensuring linearity over each gain range (TASC has four gain ranges for each channel), and provides a seamless transition between neighboring gain ranges. Temporal gain variations occurring during long time observations are also corrected for in the calibration procedure [6]. The errors at each calibration step, such as the correction of position and temperature dependence, consistency between energy deposit peaks of non-interacting protons and helium, linear fit error of each gain range and gain ratio measurements, as well as slope extrapolation, are included in the estimation of the energy resolution. As a result, a very high resolution of 2% or better is achieved above 20 GeV [13]. It should be noted that even with such a detailed calibration, the determining factor for the energy resolution is the calibration uncertainty, as the intrinsic resolution of CALET is ∼1% as for DAMPE [14]. Intrinsic resolution refers to the detector's capability by design, taking advantage of the thick fully-active total absorption calorimeter. Also important is the fact that the calibration error in the lower gain ranges is crucial for the spectrum measurements in the TeV range.

We use the "electromagnetic shower tracking" algorithm [15] to reconstruct the shower axis of each event, taking advantage of the electromagnetic shower shape and IMC design concept. As input for the electron identification, well-reconstructed and well-contained single-charged events are preselected by (1) an offline trigger confirmation, (2) geometrical condition, (3) a track quality cut to ensure reconstruction accuracy, (4) charge selection using CHD, (5) longitudinal shower development and (6) lateral shower containment consistent with those expected for electromagnetic cascades. The geometrical condition in our analysis is divided into 4 categories (A, B, C, D), depending on which detector components are penetrated by the shower axis, explained in detail in Fig. 1 of the Supplemental Material [16] and its caption. In brief, A+B are fully-contained events, while category C adds events incident from the IMC sides, and D adds events exiting through the sides of TASC. For events not crossing the CHD, we use the energy deposit of the first hit IMC layer to determine their charge.

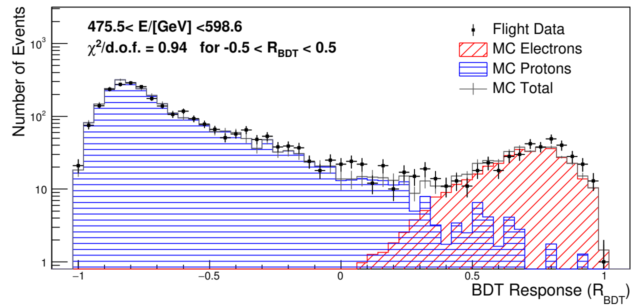

FIG. 2. An example of BDT response distributions in the 476 $< E <$ 599 GeV bin including all acceptance conditions A, B, C and D. The BDT response distributions for the TeV region are shown in Fig. 2 of the Supplemental Material [16].

The energy of incident electrons is reconstructed using the energy correction function, which converts the energy deposit information of TASC and IMC into primary energy for each geometrical condition. In order to identify electrons and to study systematic uncertainties in the electron identification, we applied two methods: a simple two parameter cut and a multivariate analysis based on boosted decision trees (BDT). The details concerning these methods are explained in the supplemental material of Ref. [6].

Calculation of event selection efficiencies, BDT training, and estimation of proton background contamination are carried out separately for each geometrical condition, and combined in the end to obtain the final spectrum. Considering the fact that the lower energy region is dominated by systematics in our analysis and therefore more statistics would not significantly improve the precision of our data, the acceptance conditions C and D are only included in the higher energy region above 475 GeV. An example of a BDT response distribution including all acceptance conditions is shown in Fig. 2. In the final electron sample, the resultant contamination ratios of protons are ∼5% up to 1 TeV, and 10%–20% in the 1–4.8 TeV region, while keeping a constant high efficiency of 80% for electrons. The number of electron candidates in the highest energy bin is 7.

The absolute energy scale was calibrated and shifted by +3.5% [6] as a result of a study of the geomagnetic cutoff energy [17]. Since the full dynamic range calibration [13] was carried out with a scale-free method, its validity holds regardless of the absolute scale uncertainty.

SYSTEMATIC UNCERTAINTIES

As discussed in detail in Ref. [6] and its Supplemental Material, systematic uncertainties in our flux measurements can be divided into three categories, i.e., energy scale uncertainty, absolute normalization, and energy dependent uncertainties. As per the energy dependent systematics, we have identified the following contributions: trigger efficiency (below 30 GeV), BDT stability, tracking, charge identification, electron identification, and MC model dependence.

BDT stability is evaluated from the stability of the resultant flux for 100 independent training samples and for BDT cut efficiency variation from 70% to 90% in 1% steps for each corresponding test sample. Upper and lower panels of Fig. 2 in the Supplemental Material [16] show an example for the stability of the BDT analysis in the $949 < E < 1194$ GeV bin and its energy dependence, respectively, where good stability over a wide range of efficiency factors and number of training samples is demonstrated. Dependence on tracking, charge identification, electron identification and MC model is estimated by using the difference of the resultant flux between representative algorithms/methods, i.e., electromagnetic shower tracking vs combinatorial Kalman filter tracking [18] algorithms, CHD vs IMC charge identification methods, simple two parameter cut vs BDT cut, and the use of EPICS vs Geant4, respectively. The obtained energy dependence of the relative flux difference in each case is fitted with a suitable log-polynomial function to mitigate statistical fluctuations as shown in Fig. 3 of the Supplemental Material [16]. Systematic effects up to a few percent are seen in the energy range below the TeV region. Statistical fluctuations are the most important limiting factor for estimating systematic errors in the TeV region, as indicated by the changes in the energy dependence of the MC model comparison from the previous publication [6]. By adding a factor of two more statistics in the highest energy region, the deviation in the 2–3 TeV bin changed significantly from the previous estimate, though by a smaller extent than the statistical error on the flux.

Since other selections, such as the track quality cut and shower concentration cuts, did not have a significant energy dependence, they were treated as uncertainties in the absolute normalization. Their contribution to the uncertainty in the absolute normalization was determined to be a very small part of the total. The total uncertainty in the absolute normalization was estimated to be 3.2%. Detailed breakdown of this uncertainty is given in the supplemental material of Ref. [6]. The high-energy trigger efficiency was verified by using data obtained with the low-energy trigger (1 GeV threshold) in the low rigidity cutoff region below 6 GV. By comparing the flux with and without offline trigger confirmation, the systematic uncertainty from trigger efficiency is estimated to be 2.4% below 30 GeV, mainly limited by the available low-energy triggered data, and is negligible above this energy. The resultant flux for each of the acceptance conditions used in this analysis is consistent within the statistical uncertainty, indicating that there are no significant systematic deviations among the acceptance conditions.

ELECTRON + POSITRON SPECTRUM

Figure 3 shows the extended electron and positron spectrum obtained with CALET using the same energy binning as in our previous publication, except for adding one extra bin at the high energy end. The error bars along horizontal and vertical axes indicate bin width and statistical errors, respectively. The gray band is representative of the quadratic sum of statistical and systematic errors, using the same definition as the one in Ref. [6]. Systematic errors include errors in the absolute normalization and energy dependent ones, except for the energy scale uncertainty. The energy dependent errors include those obtained from BDT stability, trigger efficiency in low energy region, tracking dependence, dependence on charge and electron identification methods and MC model dependence. In more refined interpretation studies, the latter four contributions could be treated as nuisance parameters while the first two components must be added in quadrature to the statistical errors. Conservatively, all of them are included in the total error estimate in Fig. 3. The measured all-electron flux including statistical errors and a detailed breakdown of the systematic errors into their components is tabulated in Table 1 of the Supplemental Material [16].

Comparing with other recent experiments (AMS-02, Fermi-LAT and DAMPE), our spectrum shows good agreement with AMS-02 data below 1 TeV. In the energy region from 40 GeV to 300 GeV, the power-law index of CALET's spectrum is found to be -3.12 ± 0.02, which is consistent with other experiments within errors. However, the spectrum is considerably softer from 300 GeV to 600 GeV than the spectra measured by DAMPE and Fermi-LAT. The CALET results exhibit a lower flux than those of DAMPE and Fermi-LAT from 300 GeV up to near 1 TeV. In this region, a difference is noticeable between two groups of measurements with internal consistency within each group: CALET and AMS-02 versus Fermi-LAT and DAMPE, indicating the presence of unknown systematic effects.

In Fig. 4 we have adopted exactly the same energy binning as DAMPE to show our spectrum. The tabulated flux for this energy binning with a detailed breakdown of systematics is also shown in Table 2 of the Supplemental Material [16]. To check if the CALET spectrum is consistent with a possible break at 0.9 TeV as suggested by DAMPE's observations, we fit our spectrum

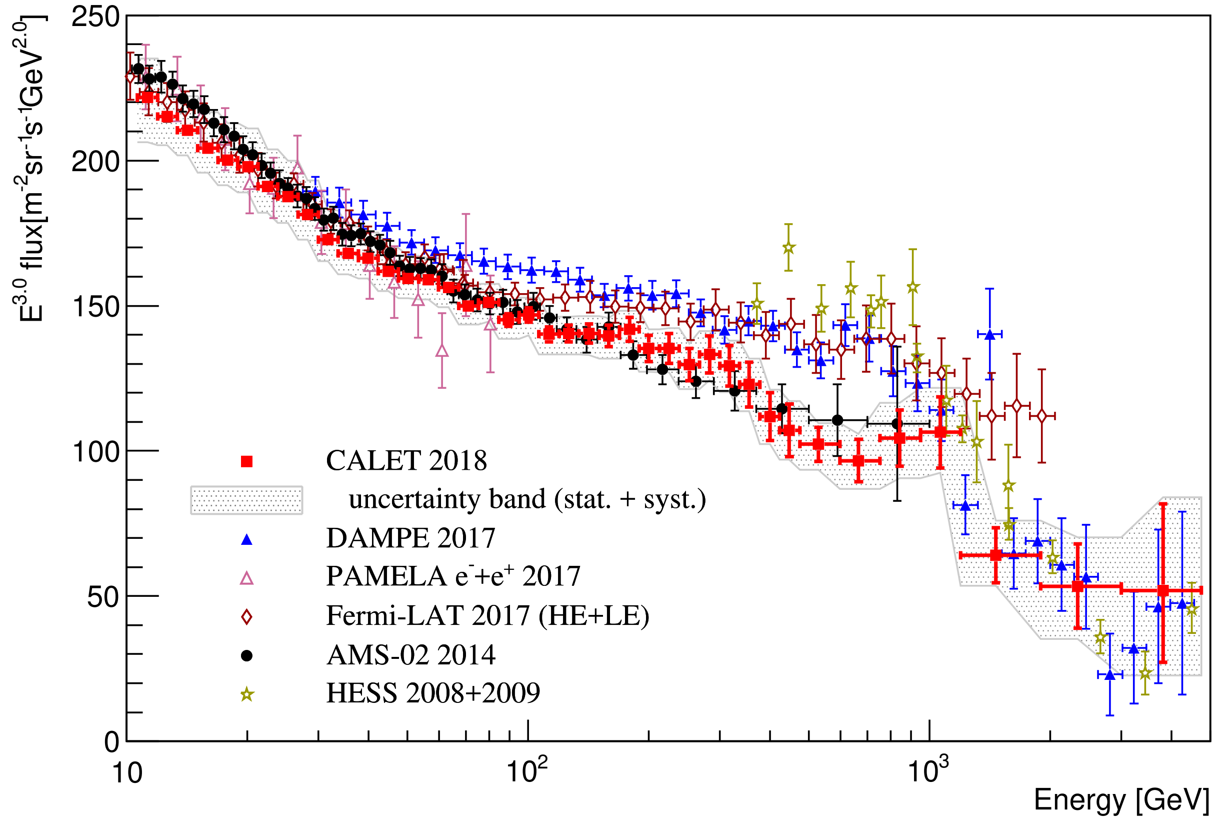

FIG. 3. Cosmic-ray all-electron spectrum measured by CALET from 10.6 GeV to 4.75 TeV using the same energy binning as in our previous publication [6], where the gray band indicates the quadratic sum of statistical and systematic errors (not including the uncertainty on the energy scale). Also plotted are direct measurements in space [7, 19–21] and from ground-based experiments [22, 23].

with a smoothly broken power law model [7] in the energy range from 55 GeV to 2.63 TeV, while fixing the break energy at 914 GeV. A broken power law steepening from -3.15 ± 0.02 to -3.81 ± 0.32 fits our data well, with $\chi^2 = 17.0$ and number of degrees of freedom (NDF) equal to 25; this result is consistent with DAMPE regarding the spectral index change of 0.7 ± 0.3. However, a single power law fit over the same energy range gives an index -3.17 ± 0.02 with $\chi^2/\mathrm{NDF} = 26.5/26$, not a significantly poorer goodness of fit than obtained with the broken power law. The fitting results are shown in Fig. 5 of the Supplemental Material [16], including a fit with an exponentially cut-off power law [20].

On the other hand, the flux in the 1.4 TeV bin of DAMPE's spectrum, which might imply a peak structure, is not compatible with CALET results at a level of 4 σ significance, including the systematic errors from both experiments. Since a sharp peak in a single bin could be an artifact due to binning effects, we have studied this kind of effect as shown in Fig. 6 of the Supplemental Material [16] and explained in its caption. The result of this study excludes with good significance the hypothesis of the presence of a peak-like structure in our data. Furthermore, bin-to-bin migration and related effects are found to be negligible when compared with our estimated systematic uncertainties.

In conclusion, we extended our previous result [6] on the CALET all-electron spectrum both in energy (to 4.8 TeV) and in acceptance, with an approximate increase by a factor two of the statistics in the higher energy region. The data in the TeV region show a suppression of the flux compatible with the DAMPE results. However, the accuracy of the break's sharpness and position, and of the spectral shape above 1 TeV, will improve by better statistics and a further reduction of the systematic errors based on the analysis of additional flight data during the ongoing 5-year (or more) observation. By specifying the breakdown of systematic uncertainties, our extended all-electron spectrum together with the AMS-02 positron flux measurement [24] provide essential information to

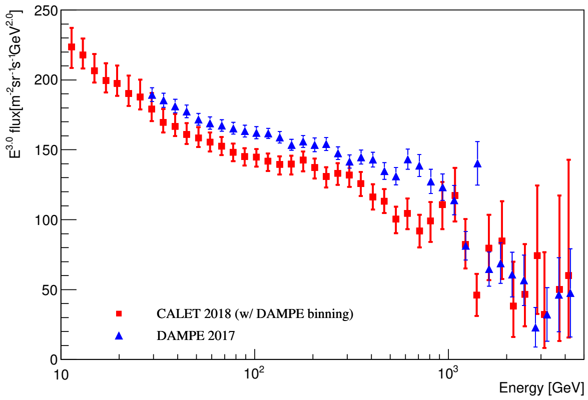

FIG. 4. Cosmic-ray all-electron spectrum measured by CALET from 10.6 GeV to 4.57 TeV using the same energy binning as the DAMPE's result [7] and compared with it. The error bars indicate the quadratic sum of statistical and systematic errors (not including the uncertainty on the energy scale).

investigate spectral features in the framework of pulsars and/or dark matter inspired models.

ACKNOWLEDGMENTS

We gratefully acknowledge JAXA's contributions to the development of CALET and to the operations onboard the ISS. We also wish to express our sincere gratitude to ASI and NASA for their support of the CALET project. This work was supported in part by a JSPS Grant-in-Aid for Scientific Research (S) (no. 26220708) and by the MEXT-Supported Program for the Strategic Research Foundation at Private Universities (2011-2015) (No. S1101021) at Waseda University. The CALET effort in the United States is supported by NASA through grants NNX16AB99G, NNX16AC02G, and NNH14ZDA001N-APRA-0075.

* yoichi.asaoka@aoni.waseda.jp
† torii.shoji@waseda.jp

[1] J. Nishimura *et al.*, Astrophys. J. **238**, 394 (1980).
[2] T. Kobayashi, Y. Komori, K. Yoshida, and J. Nishimura, Astrophys. J. **601**, 340 (2004).
[3] O. Adriani *et al.*, Nature **458**, 607 (2009).
[4] L. Accardo *et al.*, Phys. Rev. Lett. **113**, 121101 (2014).
[5] S. Torii *et al.*, in *Proceeding of Science (ICRC2015) 581* (2015).
[6] O. Adriani *et al.*, Phys. Rev. Lett. **119**, 181101 (2017).
[7] G. Ambrosi *et al.*, Nature **552**, 63 (2017).
[8] Y. Asaoka, Y. Ozawa, S. Torii, *et al.*, Astroparticle Physics **100**, 29 (2018).
[9] K. Kasahara, in *Proc. of 24th international cosmic ray conference (Rome, Italy)*, Vol. 1 (1995) p. 399.
[10] K. Kasahara, http://cosmos.n.kanagawa-u.ac.jp/EPICSHome/ (EPICS Home Page).
[11] S. Agostinelli *et al.*, Nucl. Instrum. Methods Phys. Res. **A506**, 250 (2003).
[12] http://sroesler.web.cern.ch/sroesler/dpmjet3.html (DPMJET3 Home Page).
[13] Y. Asaoka, Y. Akaike, Y. Komiya, R. Miyata, S. Torii, *et al.*, Astroparticle Physics **91**, 1 (2017).
[14] J. Chang *et al.*, Astroparticle Physics **95**, 6 (2017).
[15] Y. Akaike *et al.*, in *Proc. of 33rd international cosmic ray conference (ICRC2013) 726* (2013).
[16] See the Supplemental Material at URL for supporting figures and the tabulated all-electron fluxes in two energy binnings.
[17] M. Ackermann *et al.*, Astroparticle Physics **35**, 346 (2012).
[18] P. Maestro, N. Mori, *et al.*, in *Proceedings of Science (ICRC2017) 208* (2017).
[19] O. Adriani *et al.*, La Rivista del Nuovo Cimento **40**, 473 (2017).
[20] S. Abdollahi *et al.*, Phys. Rev. D **95**, 082007 (2017).
[21] M. Aguilar *et al.*, Phys. Rev. Lett. **113**, 221102 (2014).
[22] F. Aharonian *et al.*, Phys. Rev. Lett. **101**, 261104 (2008).
[23] F. Aharonian *et al.*, Astron Astrophys. **508**, 561 (2009).
[24] M. Aguilar *et al.*, Phys. Rev. Lett. **113**, 121102 (2014).